Posted on 16 Feb 2024 — The copyright holder is the author/funder. All rights reserved. No reuse without permission. — https://doi.org/10.22541/essoar.170808428.80423602/v1 — This is a preprint and has not been peer-reviewed. Data may be preliminary.

# An energy and enstrophy constrained parameterization of barotropic eddy potential vorticity fluxes

Rosie E Eaves[1], James R Maddison[2], David P Marshall[2], and Stephanie Waterman[3]

[1]Department of Physics, University of Oxford
[2]School of Mathematics and Maxwell Institute for Mathematical Sciences, The University of Edinburgh
[3]Department of Earth, Ocean and Atmospheric Sciences, University of British Columbia

February 16, 2024

# An energy and enstrophy constrained parameterization of barotropic eddy potential vorticity fluxes.

Rosie E. Eaves,[a] James R. Maddison,[b] David P. Marshall,[b] and Stephanie Waterman,[c]

[a] *Department of Physics, University of Oxford, Oxford, UK.*

[b] *School of Mathematics and Maxwell Institute for Mathematical Sciences, The University of Edinburgh, Edinburgh, UK.*

[c] *Department of Earth, Ocean and Atmospheric Sciences, University of British Columbia, Vancouver, British Columbia, Canada.*

*Corresponding author*: Rosie Eaves, rosie.eaves@physics.ox.ac.uk

ABSTRACT: A parameterization for barotropic eddy potential vorticity fluxes is introduced which applies both an energetic and an enstrophetic constraint to down-gradient PV mixing. An eddy kinetic energy budget and an eddy potential enstrophy budget are employed to constrain the parameterized eddy PV fluxes. The parameterization is tested for freely-decaying turbulence over variable bottom topography. Results of the simulations show that the parameterization can convert energy from the parameterized eddies to the mean flow. Furthermore, the kinetic energy and potential enstrophy budgets employed are sufficient to constrain the large-scale flow such that no spurious source of energy is introduced. As a result, the parameterization is able to produce a topography-following flow of the correct order of magnitude when compared with a high-resolution simulation.

SIGNIFICANCE STATEMENT: Small-scale eddies in the ocean, the analogue of atmospheric weather systems, are an important factor in determining the large-scale flow. In particular, in regions where the height of the ocean floor varies, eddies drive the flow towards a structure which resembles that of the ocean floor. Current methods of representing eddies in climate models are unable to capture the latter process because they fail to represent accurately the underlying physical processes that constrain the eddies. Here we present a new method for representing ocean eddies in climate models which uses conservation of energy, and of a similar quantity that measures the amount of turbulent stirring, to constrain the feedback of the eddies on the large-scale flow. We test the new method experimentally in a simple computational ocean model, analysing both the parameters that are important in the underlying physics and the large-scale flows produced by the eddies.

## 1. Introduction

Topography-following flows dominate the flow structure in the Arctic Ocean (Nand Isachsen 2003), a region which plays a crucial role in the global ocean circulation (Wang et al. 2018) and, as such, is influential in both global and localized climates. Bretherton and Haidvogel (1976) first outlined a mechanism through which turbulence drives the flow to a topography-following state. It is well known that the ocean interior is dominated by geostrophic turbulence, in which kinetic energy is cascaded to large scales while potential enstrophy is cascaded to small scales where it is dissipated. Bretherton and Haidvogel (1976) argued that eddies dissipate potential enstrophy while conserving total energy. Consequently, freely-decaying turbulence tends towards a minimum potential enstrophy state for a given initial energy, in which streamlines follow the topography contours. Crucially, these flows arise as a result of the turbulent cascades and hence they are eddy-driven. Since eddies are parameterized in the majority of CMIP6 models with an ocean component (Eyring et al. 2016; Gregory et al. 2016; Griffies et al. 2009, 2016; Jones et al. 2016), the ability of climate models to simulate eddy-driven topography-following flows is reliant on that of the eddy parameterization employed. Since the theoretical argument for the development of topography-following flows begins with the fact that eddies dissipate potential enstrophy while conserving total energy, it is sensible to suggest that an eddy parameterization which can produce realistic topography-following flows must also have these properties.

One method of parameterizing eddy-driven topography-following flows is the Neptune parameterization (Holloway 1992). Based on the idea of maximum entropy production, Holloway (1992) used the cascades of energy and enstrophy inherent to the flow to derive a solution for the flow field with maximised entropy. The Neptune parameterization relaxes the resolved flow towards a simplified estimate of this maximum entropy flow field, which follows topographic contours. Neptune has been implemented and tested in both a global (Eby and Holloway 1994) and Arctic regional (Nazarenko et al. 1998) model. In both studies, it was found that inclusion of Neptune led to flow fields which are more in agreement with observations than simulations without Neptune. For example, the inclusion of the parameterization results in the production of poleward eastern boundary undercurrents and equatorward western boundary undercurrents (Eby and Holloway 1994), as well as a more complicated surface and sub-surface flow field including a cyclonic flow in the Makarov Basin, anticyclonic flow around the Chuchki Plateau, and a returning flow along the Lomonosov Ridge (Nazarenko et al. 1998). However, Eby and Holloway (1994) noted that there were instances where the abyssal flow produced by Neptune may have been too strong, resulting in, for example, a reversed depth-integrated total transport of the California Current system. These studies highlight how the inclusion of eddy-driven topography-following flows can lead to a more accurate representation of the large-scale circulation. However, implementation Neptune in climate models is rare.

The prevailing eddy parameterization in CMIP6 models is Gent and McWilliams (1990) (hereafter referred to as GM90). GM90 parameterizes the eddy-induced transport arising from the eddy buoyancy fluxes as a prescribed advection of tracers, resulting in an adiabatic flattening of isopycnals. Through this process, energy is converted from potential energy in the large-scale[1] flow to eddy energy, thus mimicking the effects of baroclinic instability. Physically, this results in a flattening of isopycnals. Whilst the implementation of GM90 into climate models has led to many improvements (Danabasoglu et al. 1994), there are some limitations. GM90 assumes flat topography, resulting in flattened isopycnals regardless of the topographic structure, and hence leads to an unrealistic state of rest over variable bottom topography (Adcock and Marshall 2000). Additionally, the eddy energy converted from potential energy by GM90 is lost and no longer

[1]In the context of eddy parameterizations, the terms large-scale and eddy are used to signify the resolved and unresolved dynamics respectively.

accounted for in the system. In reality, quasi-geostrophic theory predicts that part of this eddy energy should cascade to larger scales (Rhines 1975) and can therefore have a direct impact on the large scale flow. GM90 provides no such mechanism for this to occur and therefore introduces a spurious sink of energy into the system. Hence, GM90 does not conserve energy.

An alternative method for parameterizing mesoscale ocean eddies is that of potential vorticity (PV) mixing, in which the eddy PV fluxes are parameterized as fluxing PV down the mean PV gradient (Green 1970; Marshall 1981). High-resolution numerical experiments have demonstrated that the eddy-induced transport correlates with isopycnic gradients of PV (Marshall et al. 1999), providing an argument for PV mixing over GM90. One advantage of PV mixing as a method of eddy parameterization is that, over variable bottom topography under freely-decaying turbulence, the large scale flow will tend to a topography-following state. To demonstrate why this is true, consider the thought experiment in Figure 1 in which a barotropic fluid layer on an $f$-plane in the northern hemisphere with a rigid lid lies over a topographic formation. We assume there is no forcing or damping in the domain, i.e. conditions of freely-decaying turbulence. If we assume the initial flow field has no systematic structure in mean relative vorticity, i.e. $\overline{\xi} = 0$ everywhere, then the structure of the mean PV is entirely determined by the spatial structure of depth, H. Thus we have large mean PV over the mount (where H is small), and low mean PV around the mount (where H is large). A down-gradient PV mixing parameterization will flux PV from areas of large mean PV to areas of low mean PV. In this scenario, the only way that mean PV can be conserved following the flow is if $\overline{\xi}$ decreases over the mount and increases around the mount, resulting in the development of a mean circulation along lines of constant depth of topography. However, when $\kappa_{\mathrm{PV}}$ is constant, i.e. an unconstrained PV mixing parameterization, the mean flow will increase in strength until PV is uniform throughout the domain, requiring an increase in energy from that of the initial state. Hence, an unconstrained down-gradient PV mixing parameterization introduces a spurious source of energy into the system and does not conserve energy (Adcock and Marshall 2000).

More recent developments in the design of eddy parameterizations have focused on developing energetically consistent parameterizations via the incorporation of an eddy energy budget.

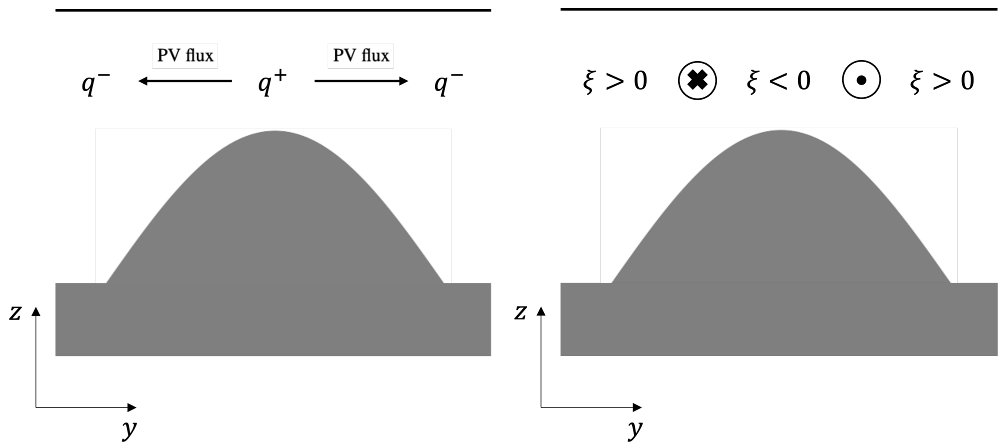


FIG. 1. A thought experiment to demonstrate how down-gradient PV mixing leads to a topography-following flow. Left panel shows the PV flux as a result of a barotropic fluid on an $f$-plane in the northern hemisphere with a rigid lid lying over a topographic formation and in which there is no systematic structure in the mean relative vorticity, i.e. $\overline{\xi} = 0$ everywhere. In such a case, the PV gradient is determined by the spatial structure of H and a down-gradient PV mixing scheme will act to flux PV from the region over the mount (where PV is large) to the region around the mount (where PV is small). Panel on the right shows the flow as a result of the PV flux indicated in the left panel. Relative vorticity increases in the region around the mount and decreases in the region over the mount, resulting in a circulation along lines of constant topographic depth.

The budget calculates the eddy energy in the system which is then used to inform the eddy parameterization and hence the mean flow. For example, Cessi (2008) and Eden and Greatbatch (2008) incorporated an eddy kinetic energy (EKE) budget into GM90 by combining it with mixing length arguments to determine the eddy diffusivity parameter. Whilst this makes the mean flow energetically consistent with the eddy flow, there is still no mechanism through which EKE can cascade to resolved scales and hence the system is not energy conserving. Bachman (2019) proposed a framework for such a mechanism which re-injects the EKE converted from potential energy by GM90 back into the larger scale barotropic flow via negative diffusion. This results in an improved kinetic energy spectrum at large scales. However, all of these approaches fundamentally rely on using GM90; as a result, they lead to flat isopycnals when implemented over varying topography thus failing to produce a topography-following flow.

Marshall and Adcroft (2010) developed an energetically constrained PV mixing parameterization by applying the methods of Eden and Greatbatch (2008) to the PV mixing parameterization framework. By incorporating an energy budget, this approach was able to constrain the effect of the parameterized eddies on the large-scale flow such that it no longer generated a spurious source of energy. Furthermore, they demonstrated that when the eddy PV fluxes are represented as down-gradient PV mixing the growth or decay of the instabilities of the flow was described by a parameterized analogue of Arnold's first stability theorem (Arnold 1965). However, this parameterization was tested in a domain with flat topography and it remains to be determined if such a parameterization conserves energy when topography is introduced.

Another issue related to energy conservation in coarse resolution models is that part of the inverse kinetic energy cascade remains unresolved. This means that kinetic energy at unresolved scales cannot cascade to the larger resolved scales as is typical of geostrophic turbulence. Attempts have been made to parameterize this transfer of energy from unresolved to resolved scales. For example, Jansen and Held (2014) developed such a parameterization which returned the energy dampened at the grid-scale by explicit viscosity back to the resolved flow via a forcing term in the governing equations. The forcing was applied both randomly (using Gaussian noise) and through the use of a negative Laplacian. Mana and Zanna (2014) developed a stochastic parameterization for eddies which represents the effect of the eddies via the divergence of a non-Newtonian stress which was shown to backscatter energy in a wind-driven gyre setup (Zanna et al. 2017). Both studies found that their respective parameterizations led to an improved kinetic energy spectra at all scales (Jansen and Held 2014; Zanna et al. 2017).

The GEOMETRIC framework (Marshall et al. 2012) is an alternative energetically-constrained parameterization that is based on the decomposition of eddy momentum fluxes into components based on eddy geometry and eddy energy. In the implementation of the GEOMETRIC framework as a parameterization, the eddy energy is solved for prognostically via an energy budget. The geometric parameters, which must be specified, are non-dimensional and strongly bounded in magnitude, making them easier to specify. These parameters also have strong connections with classical stability theory (Marshall et al. 2012; Tamarin et al. 2016). We adopt a similar approach in this study.

In this paper, we present a new formulation of a barotropic PV mixing parameterization which incorporates an eddy potential enstrophy budget in addition to an EKE budget. The resulting parameterization is therefore both energetically and enstrophetically consistent and the parameterized eddy PV fluxes are constrained by both the eddy potential enstrophy and the EKE. Since the kinetic energy and potential enstrophy cascades are both important factors in the theory underpinning eddy-driven topography-following flows, we hypothesize that incorporating budgets for both will suffice to constrain the down-gradient PV mixing parameterization such that it no longer violates the law of energy conservation when implemented over topography. We test and demonstrate the functionality of the parameterization through a set of highly idealised experiments.

The rest of this article is structured as follows. In section 2, we outline the formulation of the new energetically- and enstrophetically-constrained down-gradient PV mixing parameterization. In section 3, we describe our methods related to testing this parameterization in an idealised model, including the experimental design and details about the numerical model set-up. In section 4, we compare the results of a barotropic spin-down experiment with random topography at eddy-resolving resolution with that of a coarse resolution simulation in which no parameterization is employed in order to highlight what is required of the parameterization for this problem. In section 5, we present the results of experiments designed to demonstrate the functionality of the parameterization. Finally, in section 6, we summarise and discuss the work presented here as well as avenues for future work.

## 2. A new parameterization for eddy potential vorticity fluxes

This section outlines a new formulation of a down-gradient PV mixing parameterization as a method for parameterizing the eddy PV fluxes that is both energetically and enstrophetically constrained.

### a. Down-gradient potential vorticity mixing parameterizations

Down-gradient PV mixing parameterizations parameterize the eddy PV fluxes as mixing PV down the mean PV gradient at a specified rate controlled by an eddy diffusivity. This takes the form

$$\overline{q'\mathbf{u}'} = -\kappa_{\mathrm{PV}} \nabla \overline{q}, \tag{1}$$

where $\mathbf{u}$ is the horizontal velocity with components $u$ and $v$ in the zonal ($x$) and meridional ($y$) directions respectively, $\kappa_{\mathrm{PV}}$ is the eddy PV diffusivity, and $q$ is the PV, defined for a barotropic fluid as

$$q = \frac{f + \xi}{\mathrm{H}} \tag{2}$$

where $f$ is planetary vorticity, $\xi$ is relative vorticity, defined as $\xi = \partial v/\partial x - \partial u/\partial y$, and H is layer depth[2]. In Equation (1), and throughout the rest of this paper, overbars denote a time-mean, used to represent the large-scale, slowly evolving component of the flow, and primes denote a deviation from the time-mean, used to define the eddy component of the flow.

### b. Constraining the eddy potential vorticity fluxes

To constrain the eddy PV fluxes, $\overline{q'\mathbf{u}'}$, we exploit the following bound:

$$|\overline{q'\mathbf{u}'}|^2 \leq 4\Lambda K, \tag{3}$$

where $\Lambda$ is the eddy potential enstrophy and $K$ is the eddy kinetic energy, defined as

$$\Lambda = \frac{\overline{q'^2}}{2}, \tag{4}$$

and

$$K = \frac{\overline{u'^2} + \overline{v'^2}}{2}, \tag{5}$$

[2]Note that H must be invariant with time in order for Equation (1) to be true. In the experiments discussed and analysed in this paper we assume one vertical layer with a rigid lid and a bottom topography that is invariant with time. Hence, this requirement is satisfied.

respectively. The bound in Equation 3 holds, for example, for eddy-mean decomposition via time-averaging as used in this paper. We now employ a similar approach to Marshall et al. (2012) to construct a down-gradient PV mixing parameterization from Equation (3). An efficiency parameter, $\gamma_q$, can be defined from the bound in Equation (3):

$$|\overline{q'\mathbf{u}'}| = 2\gamma_q\sqrt{\Lambda K}, \tag{6}$$

where $0 \leq \gamma_q \leq 1$. Here, $\gamma_q$ describes how efficient the eddies are at fluxing PV and hence we refer to it as the PV flux efficiency parameter. When $\gamma_q = 0$, the eddy PV flux is zero on average. In this case, the eddies do not act to move the system towards a more ordered state. When $\gamma_q = 1$, the eddy PV flux magnitude is at its maximum value.

From the bound in Equation (3), we construct an energetically and enstrophetically constrained down-gradient PV mixing parameterization by letting

$$\overline{q'u'} = -2\gamma_q\sqrt{\Lambda K}\cos\phi_q, \tag{7}$$

$$\overline{q'v'} = -2\gamma_q\sqrt{\Lambda K}\sin\phi_q, \tag{8}$$

where $\phi_q$ is the angle of the vector $\nabla\overline{q}$ to the $x$-axis. This choice for $\overline{q'u'}$ and $\overline{q'v'}$ satisfies the bound in Equation (3). Since $\nabla\overline{q} = |\nabla\overline{q}|\left(\cos\phi_q, \sin\phi_q\right)$, we find that for $\nabla\overline{q} \neq 0$:

$$\overline{q'\mathbf{u}'} = -\frac{2\gamma_q\sqrt{\Lambda K}}{|\nabla\overline{q}|}\nabla\overline{q}. \tag{9}$$

Equation (9) describes a down-gradient PV mixing parameterization in which the eddy PV diffusivity is given by

$$\kappa_{\mathrm{PV}} = \frac{2\gamma_q\sqrt{\Lambda K}}{|\nabla\overline{q}|}. \tag{10}$$

A key feature of the parameterization is that the magnitude of the eddy PV fluxes are determined by both the EKE and eddy potential enstrophy in the system. Since $\kappa_{\mathrm{PV}}$ is non-negative, the choice to include a factor of -1 in Equations (7) and (8) imposes down-gradient PV mixing by design.

One caveat to this approach is that, whilst it is true that the eddies flux PV down the mean PV gradient on average (Marshall and Adcroft 2010), this is not necessarily the case locally (e.g. Waterman and Lilly, 2015). However, imposing down-gradient PV mixing is a common tactic in eddy parameterization design so we deem it a sufficient assumption for this first demonstration-of-concept exercise.

### *c. Specifying K and* $\Lambda$

It remains to determine $\Lambda$ and $K$, the eddy potential enstrophy and eddy kinetic energy respectively, for use in informing the parameterization. One strategy for determining these parameters is to specify their initial distribution and employ prognostic equations (i.e. an eddy potential enstrophy and EKE budget) to step forward $\Lambda$ and $K$ at each time step, then using the time-evolving values to inform the parameterization. This strategy ensures that the parameterization is flow-aware. The intention of this formulation is that the parameterization's dependence on time-evolving budgets of $\Lambda$ and $K$ will act to realistically constrain the energy of the resolved flow.

Following Cessi (2008), Eden and Greatbatch (2008) and Marshall and Adcroft (2010), we employ an EKE budget for a barotropic fluid. The relevant EKE equation is

$$\frac{\partial K}{\partial t} = \overline{q'\mathbf{u}'} \cdot \nabla\overline{\psi} - \frac{1}{\mathrm{H}}\nabla \cdot \mathrm{H}\overline{\mathbf{u}'B'} + \mathbf{F}_K, \tag{11}$$

where $K$ is the parameterized EKE, $\psi$ is the transport stream function, $B$ is the Bernoulli potential defined as $B = \mathbf{u}\cdot\mathbf{u}/2 + p/\rho_0$ where $p$ is the pressure and $\rho_0$ a reference density, and $\mathbf{F}_K$ represents sources and sinks of eddy kinetic energy.

The first term on the right hand side of Equation (12) represents kinetic energy conversion between the large-scale and eddy components of the flow (Marshall and Adcroft 2010) with a positive value signifying conversion from the mean flow to the eddies. The second term on the right hand side integrates to zero over the domain and therefore acts only to redistribute the energy. Following Eden and Greatbatch (2008) and Marshall and Adcroft (2010), we represent this redistribution of $K$ as advection by the depth-integrated large-scale flow and Laplacian diffusion with coefficient $\mu$. We include only a sink of $K$ through bottom friction in $\mathbf{F}_K$ which we parameterize as linear drag with coefficient $r_K$. Thus our EKE budget is

$$\frac{\partial K}{\partial t} = \overline{q'\mathbf{u}'} \cdot \nabla\overline{\psi} - \frac{1}{\mathrm{H}}\nabla \cdot (K\mathrm{H}\overline{\mathbf{u}}) - r_K K + \mu\nabla^2 K. \tag{12}$$

We also employ an eddy potential enstrophy budget. The relevant eddy potential enstrophy equation is

$$\frac{\partial \Lambda}{\partial t} = -\overline{q'\mathbf{u}'} \cdot \nabla\overline{q} - \frac{1}{\mathrm{H}}\nabla \cdot (\Lambda\mathrm{H}\overline{\mathbf{u}}) - \frac{1}{\mathrm{H}}\nabla \cdot \left(\mathrm{H}\overline{\frac{q'^2}{2}\mathbf{u}'}\right) + \mathbf{F}_\Lambda, \tag{13}$$

where $\Lambda$ is the parameterized eddy potential enstrophy and $\mathbf{F}_\Lambda$ represents sources and sinks of $\Lambda$.

The first term on the right hand side of Equation (14) represents eddy potential enstrophy generation. When $-\overline{q'\mathbf{u}'} \cdot \nabla\overline{q}$ is positive, the eddy PV flux is, on average, down the mean PV-gradient, that is, the eddies act to mix PV. This mixing of PV by the eddies results in a generation of eddy potential enstrophy. When $-\overline{q'\mathbf{u}'} \cdot \nabla\overline{q}$ is negative, the eddy PV flux is, on average, up the mean PV gradient, i.e. the eddies are acting to unmix the PV, resulting in a decrease in the eddy potential enstrophy. Due to the formulation of the parameterization, this term will always be negative in the parameterized simulations and thus acts only to mix PV. The second term on the right hand side represents the advection of eddy potential enstrophy by the depth-integrated large-scale flow. We neglect the third term on the right hand side since it is a product of three eddy terms and is thus assumed to be small. We include both damping of enstrophy at small scales and viscous diffusion in $\mathbf{F}_\Lambda$ which we represent as linear and Laplacian damping with coefficients $r_\Lambda$ and $\mu$ respectively. Thus our eddy potential enstrophy budget is

$$\frac{\partial \Lambda}{\partial t} = -\overline{q'\mathbf{u}'} \cdot \nabla\overline{q} - \frac{1}{\mathrm{H}}\nabla \cdot (\Lambda\mathrm{H}\overline{\mathbf{u}}) - r_\Lambda \Lambda + \mu\nabla^2 \Lambda. \tag{14}$$

The energetically and enstrophetically informed down-gradient PV mixing formula, the eddy kinetic energy budget and the eddy potential enstrophy budget (Equations (9), (12) and (14) respectively) describe the parameterization fully. There are four input parameters to the parameterization: the PV flux efficiency parameter, $\gamma_q$; the eddy diffusivity, $\mu$; the EKE dissipation coefficient, $r_K$;

and the eddy potential enstrophy dissipation coefficient, $r_\Lambda$. The initial distributions of EKE ($K_0$) and eddy potential enstrophy ($\Lambda_0$) must also be specified. $K$ and $\Lambda$ evolve with time through their respective budgets and the time-evolving values are then used to determine the magnitude of the down-gradient PV fluxes at each time-step. Employing energy and enstrophy budgets with spatial dependence ensures the parameterization is flow-aware. Through these budgets, the parameterization accounts for the conversion of energy from large-scale to eddy and vice versa, the dissipation of EKE by bottom friction, the generation of enstrophy through PV mixing and enstrophy dissipation at small scales.

It should be noted that Equation (9) does not satisfy the integral constraint necessary for angular momentum in a zonal channel (Marshall 1981; Marshall et al. 2012). We plan to initially test the parameterization in the case of a simply connected basin in which this integral constraint is less of a concern. Further work to satisfy this constraint is left for future work.

## 3. Methods

### *a. Experimental design*

To analyse the performance of the parameterization, we implement it in an idealised experimental set-up, with which we aim to answer the following key questions:

1. Can the parameterization convert kinetic energy from the eddy field to the large-scale flow, thus producing an eddy-driven topography-following flow?
2. Do the energetics and enstrophetics exhibit similar behaviour to their explicit counterparts in an eddy-resolving simulation?
3. How do the input parameters affect the energetics and enstrophetics of the dynamics?

To answer these questions, we run a set of numerical simulations in which we simulate barotropic freely-decaying turbulence over random topography on an $f$-plane. We choose to simulate freely-decaying turbulence over bottom topography since theory predicts that this will lead to an eddy-driven topography-following flow (Bretherton and Haidvogel 1976). We use the following four configurations:

| Code | Resolution | Eddies | $\mu_\xi$ ($\mathrm{m^{-4}s^{-1}}$) | $\gamma_q$ | $r_\Lambda$ ($\mathrm{s^{-1}}$) | $r_K$ ($\mathrm{s^{-1}}$) | $\mu$ ($\mathrm{m^{-2}s^{-1}}$) | $\kappa_{\mathrm{PV}}$ |
|---|---|---|---|---|---|---|---|---|
| 5km$_{\mathrm{EXP}}$ | 5km | Explicit | $10^8$ | - | - | - | - | - |
| 50km$_{\mathrm{EXP}}$ | 50km | Explicit | $10^{11}$ | - | - | - | - | - |
| 50km$_{\mathrm{EECON}}$ | 50km | Parameterized | $10^{11}$ | 0.1 | $4.5\times10^{-8}$ | 0 | 500 | - |
| 50km$_{\mathrm{UNCON}}$ | 50km | Parameterized | $10^{11}$ | - | - | - | - | 50 |

TABLE 1. Parameters used in the simulations analysed in Sections 4 and 5.

(a) an eddy-resolving (5km horizontal resolution) simulation with explicit eddies only (5km$_{\mathrm{EXP}}$);

(b) a coarse-resolution (50km horizontal resolution) simulation with explicit eddies only (50km$_{\mathrm{EXP}}$);

(c) a coarse-resolution simulation with parameterized eddies where we employ an unconstrained down-gradient PV mixing parameterization, i.e. with constant $\kappa_{\mathrm{PV}}$ (50km$_{\mathrm{UNCON}}$);

(d) a coarse-resolution simulation with parameterized eddies as described in Section 2, i.e. with an energetically and enstrophetically constrained down-gradient PV mixing parameterization (50km$_{\mathrm{EECON}}$).

We compare 50km$_{\mathrm{EECON}}$ with 50km$_{\mathrm{UNCON}}$ to assess if the energetic and enstrophetic constraints imposed are successful in constraining the kinetic energy of the resolved flow. We use 5km$_{\mathrm{EXP}}$ as a reference to inform on a realistic kinetic energy for the resolved flow, thus allowing us to determine if the resolved flow is well-constrained by the parameterization. We run many variations of 50km$_{\mathrm{EECON}}$ varying the input parameters to the parameterization for each simulation. The details of the simulations are outlined in Table 1.

### *b. Model equations*

In these experiments, we simulate freely-decaying turbulence in a barotropic fluid (i.e. one vertical layer) with a rigid lid. The equations of motion are the mean depth-integrated potential vorticity equation, which, for explicit eddy simulations is

$$\frac{\partial\overline{\xi}}{\partial t} = -\nabla\cdot\overline{\zeta}\,\overline{\mathbf{u}} - \mu_\xi\nabla^4\overline{\xi}, \tag{15}$$

and for parameterized eddy simulations is

$$\frac{\partial \overline{\xi}}{\partial t} = -\nabla \cdot \overline{\zeta}\,\overline{\mathbf{u}} - \nabla \cdot \overline{\zeta' \mathbf{u}'} - \mu_\xi \nabla^4 \overline{\xi}, \tag{16}$$

where the eddy PV flux term is replaced with the appropriate parameterization, and the continuity equation,

$$\nabla \cdot \mathrm{H}\overline{\mathbf{u}} = 0, \tag{17}$$

where $\zeta = f + \xi$ and $\mu_\xi$ is the biharmonic diffusion coefficient. We employ biharmonic diffusion in Equations (15) and (16) for stability.

### *c. Numerical Implementation*

The numerical implementation of time-stepping of Equations 15 and 16 are as follows. The variables are arranged with vorticity, stream function and layer depth defined at the cell vertices. The zonal and meridional components of the velocity are calculated using a centred second-order differencing scheme. We use free-slip lateral boundary conditions, i.e. $\overline{\xi} = 0$ on lateral boundaries, and no flow normal to the boundary, i.e. constant $\overline{\psi}$ on lateral boundaries. For simplicity, we choose $\overline{\psi} = 0$. Advection is calculated using an energy- and enstrophy-conserving scheme defined by Arakawa (1966). Biharmonic diffusion of vorticity is calculated using a centred differencing scheme with $\nabla^2 \overline{\xi} = 0$ on the lateral boundaries.

For parameterized simulations, $K$ and $\Lambda$ are defined at the cell centre points. We specify a no flux boundary condition for $K$ and $\Lambda$, i.e. there is no diffusion or advection of $K$ or $\Lambda$ through lateral boundaries. Time-stepping of Equations (12), (14), (15) and (16) is computed using the third order Adams-Bashforth method, with the first two time steps calculated using a first-order forward approximation.

### *d. Specification of Domain Geometry*

All simulations are run in a square domain of side length $L = 2000$km with non-flat topography. The topography is created by using a seeded pseudorandom number generator (NumPy random.default_rng) to generate independent Fourier modes using a Gaussian distribution at 5km

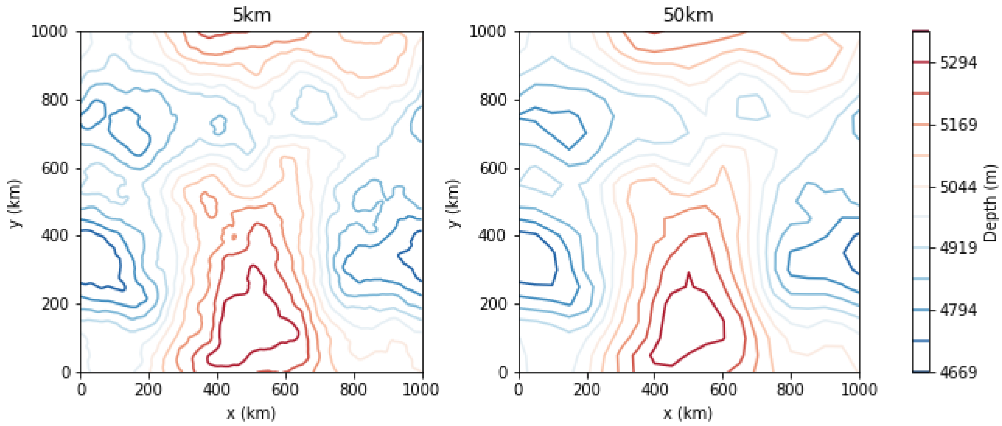


FIG. 2. Topography used in high-resolution simulations (left) and coarse resolution simulations (right).

resolution. A peak wavenumber is specified when generating the Fourier modes to ensure the topography is not confined to small-scale structures. The field generated by the Fourier modes is then multiplied by a constant and translated in depth in order to produce a topography with average depth of 5km and depth variations of around 10%. The topography is regridded using spatial averaging to 50km resolution for the coarse-resolution simulations. The topographic structure used is shown in Figure 2.

### *e. Specification of Model Parameters*

The Coriolis parameter is taken as a constant with value $f_0 = 0.7\times10^{-4}$ s$^{-1}$ in all simulations. The biharmonic diffusion coefficient, $\mu_\xi$, is set to $10^8$ m$^4$ s$^{-1}$ for simulations at 5km resolution and $10^{11}$ m$^4$ s$^{-1}$ for simulations at 50km resolution. These values are chosen to be as small as possible such that grid scale noise is no longer generated. All simulations are run for a total of 3000 days in order to reach a point at which the energy conversion from eddy to mean has plateaued.

For the coarse resolution simulation with the constrained parameterization, 50km$_{\text{EECON}}$, there are four extra parameters for which values need to be specified: the PV flux efficiency parameter, $\gamma_q$; the enstrophy damping parameter, $r_\Lambda$; the energy damping parameter, $r_K$; and the eddy diffusivity, $\mu$. Analysis of $\gamma_q$ in the high-resolution simulation gives an average value of 0.1 (not shown) and hence this value is used in 50km$_{\text{EECON}}$. The enstrophy damping parameter, $r_\Lambda$, is diagnosed from 5km$_{\text{EXP}}$ by taking the volume integral of Equation (14) and then integrating in time. The damping parameter undergoes an initial adjustment period before reaching a constant value at around 500 days (not shown). Since a constant value of $r_\Lambda$ is input to the parameterization, the value is taken as that of $5\mathrm{km}_{\mathrm{EXP}}$ after the initial adjustment period, which is $5.0\times10^{-8}$ s$^{-1}$. Since these experiments simulate freely-decaying turbulence and we do not have any damping from bottom friction in the explicit eddy simulations, we set $r_K = 0$ s$^{-1}$. Finally, the diffusivity coefficient, representing the diffusivity of parameterized EKE and eddy potential enstrophy, is set to $\mu = 500$ m$^2$ s$^{-1}$. A minimum value for $|\nabla\overline{q}|$ is specified at each time step to avoid division by zero. A maximum value for $\kappa_{\mathrm{PV}}$ is also specified at each time step.

For the coarse resolution simulation with unconstrained eddy PV fluxes, $50\mathrm{km}_{\mathrm{UNCON}}$, a constant value of $\kappa_{\mathrm{PV}}$ must be specified. We set this to the initial value of $\kappa_{\mathrm{PV}}$ in simulation $50\mathrm{km}_{\mathrm{EECON}}$ which is 100 m$^2$s$^{-1}$.

### *f. Specification of Initial Conditions*

Simulations with explicit eddies are initialised with a stream function which is generated at 5km resolution using a similar method as that of the topography. The field generated by the Fourier modes is multiplied by a constant to produce velocities of the order of $1-10$ cm s$^{-1}$. This is regridded using volume averaging to 50km resolution for coarse-resolution simulations. The initial stream functions are plotted in figure 3. In configurations with explicit eddies, since there are no forcing terms, it is assumed that the turbulent cascades of energy, and hence the eddies, are driving the large scale flow. Simulations with parameterized eddies are run with no initial stream function and, instead, the parameterized eddies initially drive the flow.

For the coarse resolution simulation with the constrained parameterization, $50\mathrm{km}_{\mathrm{EECON}}$, the initial distributions of $K$ and $\Lambda$ must be specified. For simplicity, we use constant values values $K_0$ and $\Lambda_0$ respectively. We specify $K_0$ such that the initial parameterized EKE in $50\mathrm{km}_{\mathrm{EECON}}$ is the same as the initial kinetic energy of $5\mathrm{km}_{\mathrm{EXP}}$. We therefore set $K_0$ to the volume-averaged kinetic energy at time zero in $5\mathrm{km}_{\mathrm{EXP}}$, which is $1.5\times10^{-4}$ m$^2$s$^{-2}$. $\Lambda_0$ is set to the volume-averaged value of $\Lambda$ at 500 days in $5\mathrm{km}_{\mathrm{EXP}}$, i.e. after the initial enstrophy adjustment period, which is $1.0\times10^{-20}$ m$^{-2}$s$^{-2}$.

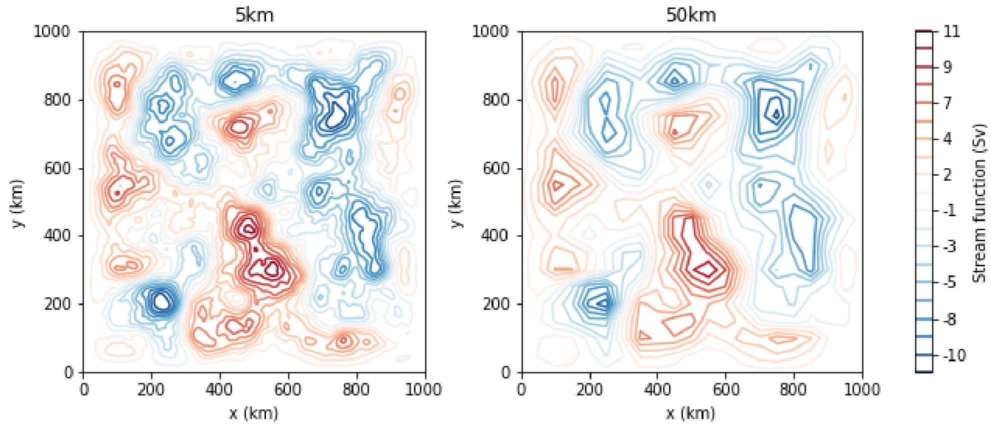


FIG. 3. Initial stream function used in simulations with explicit eddies at 5km resolution (left) and 50km resolution (right).

## 4. Explicit Eddy Simulations

We compare properties of the mean and eddy flow fields in the eddy-resolving and coarse resolution simulations, $5\mathrm{km}_{\mathrm{EXP}}$ and $50\mathrm{km}_{\mathrm{EXP}}$ respectively, to identify the unresolved eddy-driven effects on the mean/large-scale flow in the coarse resolution simulation; these effects ideally would be prescribed by the eddy parameterization. Throughout the rest of this paper, the time-mean kinetic energy (MKE), defined as $\overline{\mathbf{u}}\cdot\overline{\mathbf{u}}/2$, is used to represent the large-scale flow for all simulations. The EKE is defined as $\overline{\mathbf{u}'\cdot\mathbf{u}'}/2$ for simulations with explicit eddies. The large-scale potential enstrophy is defined as $\overline{q}\ \overline{q}/2$ for all simulations, and the eddy potential enstrophy is defined as $\overline{q'q'}/2$ for simulations with explicit eddies. All time-means are taken every 50 days over a 500 day period.

We first identify the effects of the eddies on the energetics which are unresolved in the coarse-resolution simulation and hence need to be parameterized. In $5\mathrm{km}_{\mathrm{EXP}}$, energy is converted from eddy to mean as the simulation progresses, indicated by the simultaneous decrease in EKE and increase in MKE (Figure 4a). In contrast, for $50\mathrm{km}_{\mathrm{EXP}}$, the EKE is damped throughout the simulation but the MKE does not increase and hence there is no conversion of energy from eddy to mean (Figure 4a). This is further illustrated by the eddy to mean energy conversion rate which is positive throughout the majority of the simulation in $5\mathrm{km}_{\mathrm{EXP}}$ and zero throughout the majority of the simulation in $50\text{km}_{\text{EXP}}$ (Figure 4b). Hence, we aim to parameterize the effects of this unresolved conversion on the large-scale flow i.e. to parameterize a source of large-scale kinetic energy that mimics the effects of the eddy-to-mean kinetic energy conversion present in the eddy-resolving configuration. Note that the volume averaged kinetic energy of the initial state is of a similar magnitude in both $5\text{km}_{\text{EXP}}$ and $50\text{km}_{\text{EXP}}$. However, due to the larger biharmonic diffusion coefficient in $50\text{km}_{\text{EXP}}$ than in $5\text{km}_{\text{EXP}}$, the first time-mean value is much smaller in $50\text{km}_{\text{EXP}}$ than in $5\text{km}_{\text{EXP}}$.

We now identify the effects of the eddies on the enstrophetics which are unresolved in the coarse-resolution simulation and hence need to be parameterized. In both $5\text{km}_{\text{EXP}}$ and $50\text{km}_{\text{EXP}}$ the eddy potential enstrophy decays with time and there is a large difference in magnitude between the two simulations (Figure 4c). The volume-averaged enstrophy generation term is positive throughout the simulation for $5\text{km}_{\text{EXP}}$ (Figure 4d), meaning that the eddy PV fluxes are, on average, fluxing PV down the mean PV gradient for the duration of the simulation. In $50\text{km}_{\text{EXP}}$ the enstrophy generation term is much smaller in magnitude than in $5\text{km}_{\text{EXP}}$ (Figure 4d) since the eddy field is not well resolved. Hence we require the parameterization to increase the enstrophy generation, thus increasing the magnitude of the eddy potential enstrophy. Note that here and in future sections we do not analyse the mean potential enstrophy since it is dominated by the effects of planetary vorticity and hence the effect of the parameterization on the mean potential enstrophy is negligible.

## 5. Results of Parameterized Simulations

We now analyse the results of the parameterized simulations, focusing on the four key questions outlined in Section 3.

### *a. Energy Conversion From Eddy to Mean*

The parameterization is able to convert kinetic energy from eddy to mean, shown by the simultaneous decrease in parameterized EKE and increase in MKE in $50\text{km}_{\text{EECON}}$ (Figure 5a). This is further confirmed by the parameterized energy conversion term of $50\text{km}_{\text{EECON}}$ which is positive throughout the simulation and exhibits similar behaviour in time to that of $5\text{km}_{\text{EXP}}$ (Figure 5b).

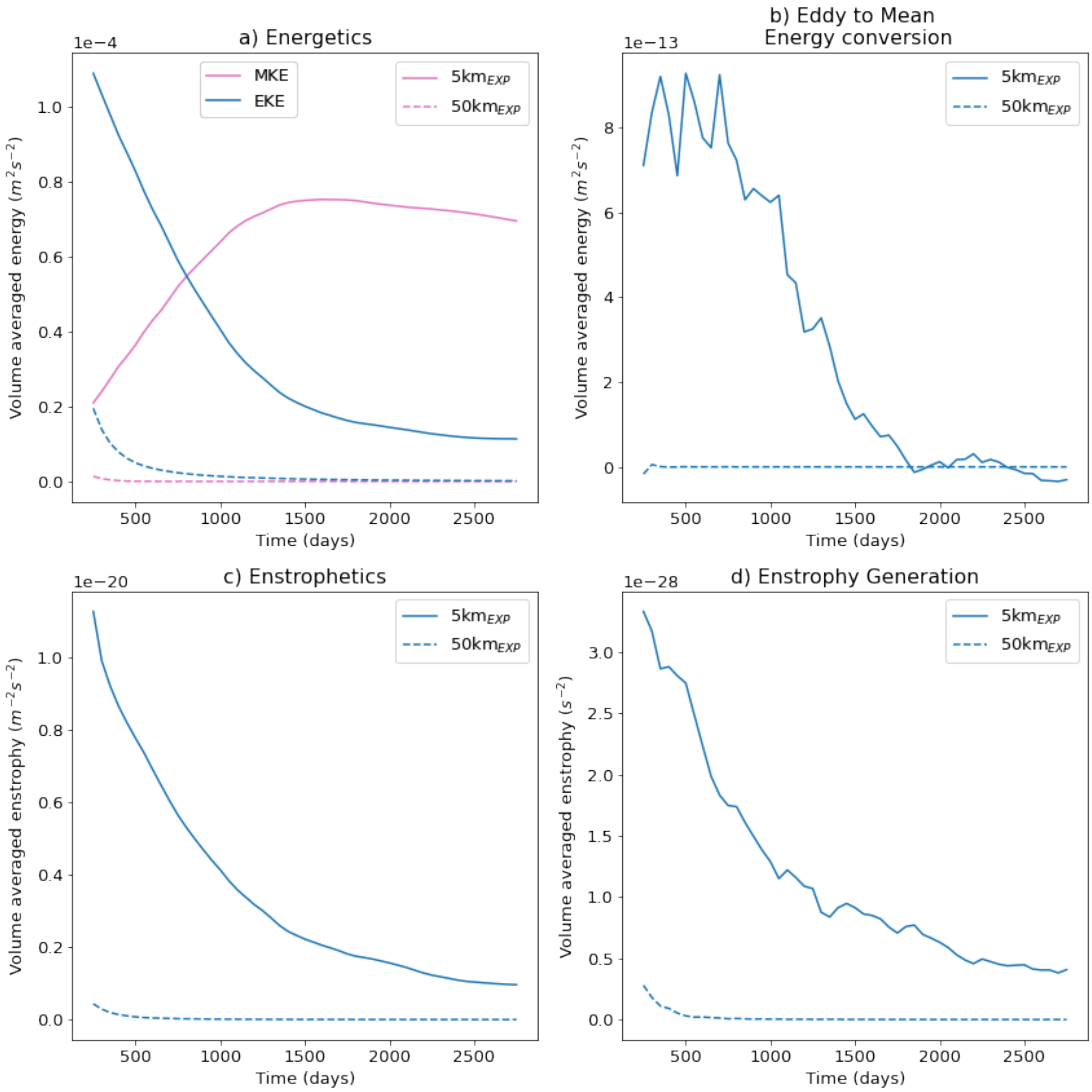


FIG. 4. Data for 5km$_{\mathrm{EXP}}$ (solid) and 50km$_{\mathrm{EXP}}$ (dashed) showing (a) rolling time-means of MKE (pink) and EKE (blue); (b) the eddy to mean energy conversion term, -$\overline{q'\mathbf{u}'} \cdot \nabla\psi$; (c) eddy potential enstrophy; (d) the enstrophy generation term, $-\overline{q'\mathbf{u}'} \cdot \nabla q$. Rolling time-means are calculated every 50 days over a 500-day period.

The parameterization is able to produce a large-scale topography-following flow as a result of the parameterized eddy-to-mean energy conversion (Figure 6).

### *b. Energetics and Enstrophetics*

We now consider the effects of the parameterization on the energetics and enstrophetics. The peak magnitudes of MKE in 5km$_{\mathrm{EXP}}$ and 50km$_{\mathrm{EECON}}$ are $7.5\times10^{-5}$ m$^2$s$^{-2}$ and $3.2\times10^{-5}$ m$^2$s$^{-2}$

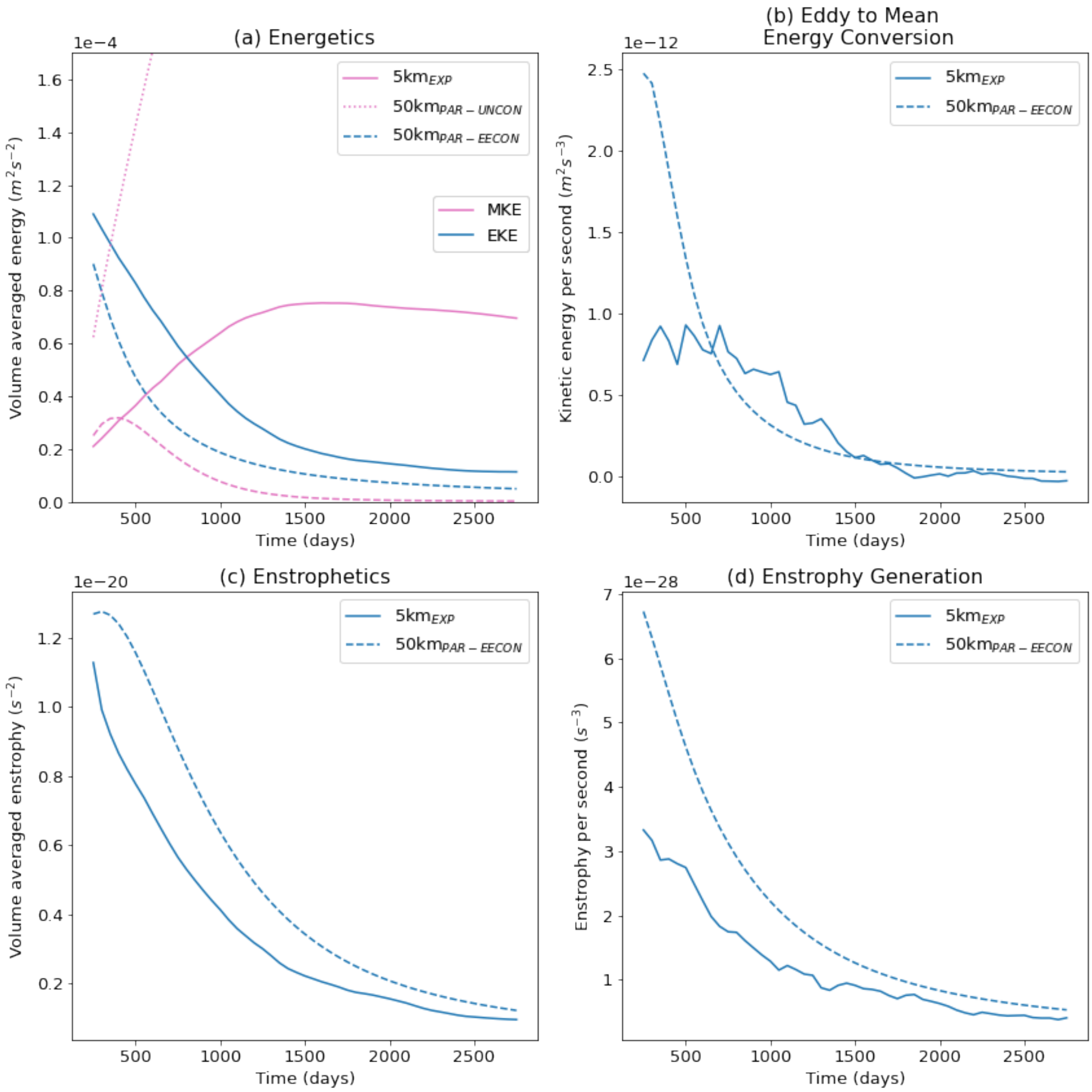


FIG. 5. Data for $5km_{EXP}$ (solid), $50km_{EECON}$ (dashed) and $50km_{UNCON}$ (dotted) showing (a) rolling time-means of MKE (pink) and EKE (blue); (b) the eddy to mean energy conversion term, $-\overline{q'\mathbf{u}'}\cdot\nabla\psi$; (c) eddy potential enstrophy; (d) the enstrophy generation term, $-\overline{q'\mathbf{u}'}\cdot\nabla q$. Rolling time-means are calculated every 50 days over a 500-day period.

respectively. Thus the parameterization leads to a peak MKE of the correct order of magnitude and with a value of 43% of that of the high-resolution simulation. In contrast, the MKE in $50km_{UNCON}$ increases throughout the simulation, reaching a magnitude almost six times greater than the maximum MKE of $5km_{EXP}$ by the end of the simulation. The difference in the magnitude of the MKE between $50km_{EECON}$ and $50km_{UNCON}$ and the similarity between $50km_{EECON}$ and

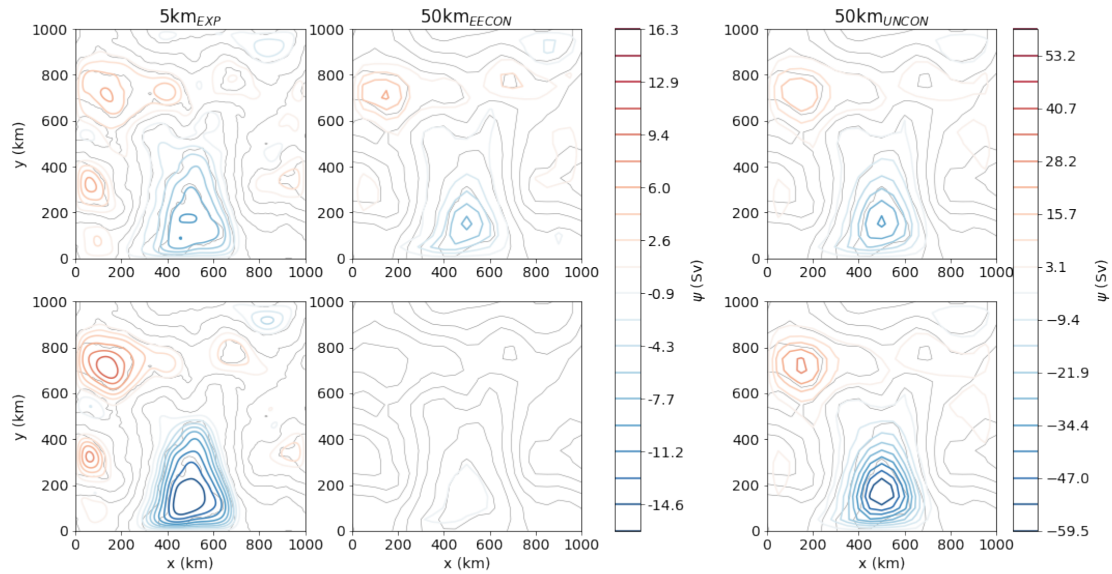


FIG. 6. Time-mean transport stream function for 5km$_{\mathrm{EXP}}$ (left), 50km$_{\mathrm{EECON}}$ (middle) and 50km$_{\mathrm{UNCON}}$ (right) over the time periods 0 - 1500 days (top) and 1501 - 3000 days (bottom). 5km$_{\mathrm{EXP}}$ and 50km$_{\mathrm{EECON}}$ are plotted on the same colour scale and 50km$_{\mathrm{UNCON}}$ is plotted using a separate colour scale for clarity. Grey lines represent topography contours as described in Figure 2.

5km$_{\mathrm{EXP}}$ suggests that the kinetic energy of the resolved flow is well-constrained by the energetic and enstrophetic constraints imposed. This is further illustrated by the magnitude of the transport stream function (Figure 6) which peaks at a value of 16.3 Sv, 8.3 Sv and 59.5 Sv in 5km$_{\mathrm{EXP}}$, 50km$_{\mathrm{EECON}}$ and 50km$_{\mathrm{UNCON}}$ respectively. Thus the peak magnitude of the transport stream function is over 250% larger than that of 5km$_{\mathrm{EXP}}$ in 50km$_{\mathrm{UNCON}}$, while it is 51% of that of 5km$_{\mathrm{EXP}}$ in 5km$_{\mathrm{EECON}}$, further demonstrating that the energetic and enstrophetic constraints imposed in 50km$_{\mathrm{EECON}}$ are indeed constraining the resolved flow.

The main difference between the energetics of 5km$_{\mathrm{EXP}}$ and 50km$_{\mathrm{EECON}}$ is the earlier, smaller peak and subsequent decaying of MKE in 50km$_{\mathrm{EECON}}$ (Figure 5a). This happens despite the fact that the eddy-to-mean energy conversion in 50km$_{\mathrm{EECON}}$ is initially larger in magnitude than that of 5km$_{\mathrm{EXP}}$ (Figure 5b). This is due to the difference in biharmonic coefficient between the simulations, which results in a larger damping of resolved kinetic energy in 50km$_{\mathrm{EECON}}$ than in 5km$_{\mathrm{EXP}}$.

Both the parameterized eddy potential enstrophy (Figure 5c) and the parameterized enstrophy generation (Figure 5d) in $50\mathrm{km}_{\mathrm{EECON}}$ are of the correct order of magnitude and both decay with time in a similar manner to that of their counterparts in $5\mathrm{km}_{\mathrm{EXP}}$. However, both are larger in magnitude than their counterparts in $5\mathrm{km}_{\mathrm{EXP}}$ throughout the simulation.

It should be noted that tuning of the input parameters in $50\mathrm{km}_{\mathrm{EECON}}$ might result in an energy conversion and enstrophy generation profile more consistent with that of $5\mathrm{km}_{\mathrm{EXP}}$; however, here we focus on the functionality of the parameterization, and do not seek to find optimally tuned parameters.

### *c. Sensitivity of the Output to Input Parameters*

We now test the sensitivity of the parameterization to the input parameters (namely $r_\Lambda$ and $\gamma_q$) and the initial conditions ($K_0$ and $\Lambda_0$) by varying these values. We find that the total energy converted from eddy to mean throughout the simulation, total potential enstrophy generated throughout the simulation, and peak MKE value all increase with increasing $\gamma_q$ and with decreasing $r_\Lambda$ (Figure 7). An increase in $\gamma_q$ increases the efficiency of the parameterized eddies to flux PV resulting in a larger eddy PV flux. Decreasing $r_\Lambda$ increases the parameterized potential enstrophy which also strengthens the eddy PV fluxes. Larger eddy PV fluxes increase PV mixing (since the eddy PV fluxes are down-gradient by design) and therefore increase enstrophy generation. Larger eddy PV fluxes also increase the magnitude of the eddy-to-mean energy conversion, resulting in a larger total amount of energy converted from eddy to mean.

The minimum values of total energy converted and total potential enstrophy generated in this experiment ($8.43\times10^{-5}$ m$^2$s$^{-2}$ and $4.41\times10^{-20}$ m$^{-1}$s$^{-1}$ respectively, Figure 7) are both larger than that of the eddy-resolving simulation ($8.26\times10^{-5}$ m$^2$s$^{-2}$ and $3.23\times10^{-20}$ m$^{-1}$s$^{-1}$ respectively, not shown). Despite this the maximum peak MKE value in this experiment ($4.03\times10^{-5}$ m$^2$s$^{-2}$, Figure 7) is smaller than the peak MKE of the eddy-resolving simulation ($7.53\times10^{-5}$ m$^2$s$^{-2}$, Figure 5a). That is, the parameterized simulations in this experiment all have a higher total energy conversion and total enstrophy generation than that of $5\mathrm{km}_{\mathrm{EXP}}$, but none are able to reach a peak MKE value as high as that of $5\mathrm{km}_{\mathrm{EXP}}$. This is again due to the difference in biharmonic coefficient between the parameterized simulations and the eddy-resolving simu-

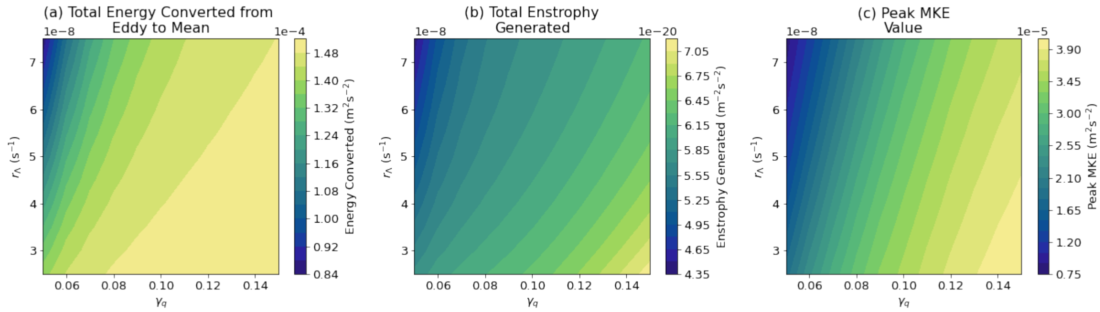


FIG. 7. Contours showing (a) total energy converted from eddy to mean; (b) total enstrophy generated; and (c) peak MKE value for a set of simulations with the same setup as $50\mathrm{km}_{\mathrm{EECON}}$ where $r_\Lambda$ and $\gamma_q$ are varied by 50% of their value in $50\mathrm{km}_{\mathrm{EECON}}$.

lation, which results in a larger damping of resolved kinetic energy in the parameterized simulations.

A similar experiment is performed varying $K_0$ and $\Lambda_0$ to test the sensitivity of the parameterization to the initial state. We find that the total energy converted from eddy to mean, total enstrophy generated and peak MKE value all increase with increasing $K_0$ (Figure 8). Increasing $K_0$ increases the magnitude of the eddy PV fluxes through Equation 9. By a similar argument to that described above, stronger eddy PV fluxes results in an increase in the total enstrophy generated and an increase in the magnitude of the energy conversion. An increase in $K_0$ also means there is more energy available in the parameterized eddies to be converted. These two things combined result in a larger total amount of energy converted from eddy to mean and hence a larger peak MKE value. In contrast, all three diagnostics show a much smaller sensitivity to $\Lambda_0$ than to $K_0$, $r_\Lambda$ or $\gamma_q$. This suggests that the strength of the eddy PV fluxes is relatively insensitive to $\Lambda_0$.

## 6. Summary and Discussion

Traditional methods of parameterizing mesoscale ocean eddies can create spurious sources or sinks of energy when implemented over variable bottom topography and can therefore fail to produce realistic eddy-driven topography-following flows. These flows arise due to the turbulent cascades of kinetic energy and potential enstrophy inherent to quasi-geostrophic flow (Bretherton and Haidvogel 1976). It is therefore sensible to suggest that, in attempting to develop a parameterization for mesoscale eddies which can produce realistic eddy-driven topography-following

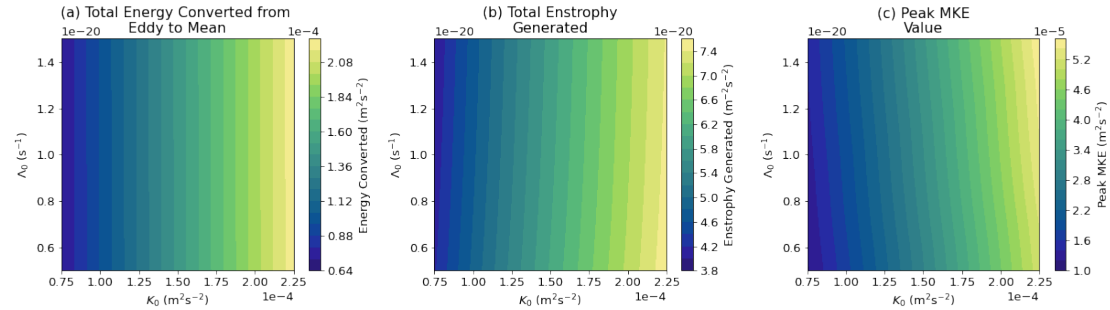


FIG. 8. Contours showing (a) total energy converted from eddy to mean; (b) total enstrophy generated; and (c) peak MKE value for a set of simulations with the same setup as $50\text{km}_{\text{EECON}}$ where $K_0$ and $\Lambda_0$ are varied by 50% of their value in $50\text{km}_{\text{EECON}}$.

flows, there should be some consideration of both the kinetic energy and the potential enstrophy. Previous work has seen a number of studies incorporating an energy budget into a mesoscale eddy parameterization (e.g. Cessi (2008); Eden and Greatbatch (2008); Marshall and Adcroft (2010); Marshall et al. (2012)) but, to our knowledge, the same focus has not been applied to the potential enstrophy.

We have presented a new parameterization for barotropic eddies which incorporates an eddy potential enstrophy budget in addition to an eddy kinetic energy budget. The parameterization imposes down-gradient PV mixing in which the strength of the eddy PV fluxes is determined by both the parameterized EKE and eddy potential enstrophy.

The EKE budget employed here includes the following terms: the energy conversion term which accounts for conversion from eddy to mean and vice versa; a dissipation term which represents bottom friction via linear damping; and a redistribution of EKE which we represent as advection by the depth-integrate large-scale flow and Laplacian diffusion. In reality, the redistribution of EKE involves a myriad of processes and our choice of representation may be considered a crude approximation. Nonetheless, we believe this choice to be sufficient as a simple approximation. The eddy potential enstrophy budget includes the following terms: the potential enstrophy generation term which accounts for enstrophy generated through mixing of PV by the parameterized eddies; a dissipation term which represents the viscous dissipation of potential enstrophy at small scales via linear damping; advection by the depth-integrated large-scale flow; and a Laplacian diffusion term. The diffusion terms in both budgets represent the diffusion of each by the eddies and hence they use the same diffusion coefficient. The strength of the parameterized eddy PV fluxes therefore depends on all of these factors. These budgets lead to the following parameters which must be specified: the EKE dissipation parameter, $r_K$; the potential enstrophy dissipation parameter, $r_\Lambda$; and the eddy diffusion coefficient, $\mu$. Additionally, the eddy PV flux efficiency parameter, $\gamma_q$, must be specified. For simplicity we have chosen to specify a constant value for $\gamma_q$, despite the fact that in reality $\gamma_q$ will likely have spatial and temporal dependence.

The parameterization has been tested in an idealised ocean basin with variable bottom topography, simulating freely-decaying turbulence on an $f$-plane. Our key findings are:

1. The parameterization is able to convert kinetic energy from eddy to mean, resulting in a large-scale topography-following flow.

2. The energetics and enstrophetics exhibit similar behaviour to that of an eddy-resolving simulation, with the main difference being an earlier, smaller peak in MKE. This is due to the difference in biharmonic diffusion coefficients in each simulation, which results in a larger damping of resolved kinetic energy in the parameterized simulation. The results suggest the inclusion of the EKE and eddy potential enstrophy budget are sufficient to produce a resolved flow with kinetic energy which is well-constrained, i.e. comparable in magnitude to that of an eddy-resolving simulation.

3. The input parameters $\gamma_q$ and $r_\Lambda$ work as expected with an increase in $\gamma_q$ and a decrease in $r_\Lambda$ resulting in a larger eddy-to-mean energy conversion. The resolved flow depends on $K_0$, the EKE of the initial state, with a larger $K_0$ resulting in a larger eddy-to-mean energy conversion. The resolved flow is relatively insensitive to $\Lambda_0$, the eddy potential enstrophy of the initial state.

The parameterization provides a mechanism through which energy can be transferred from unresolved to resolved scales and hence can backscatter energy. Currently, the source of the unresolved kinetic energy is the EKE of the initial state, whilst in other energy backscatter parameterizations it is the kinetic energy dampened at the grid scale via explicit viscosity (e.g.

Jansen and Held (2014); Mana and Zanna (2014)). The use of an EKE budget in the framework outlined here opens up the possibility of introducing other sources of EKE, which could be explored in future work.

There are some significant limitations to the parameterization as it is in its current form. Firstly, it is a known problem that, in a multiply-connected domain, integral constraints on the eddy PV fluxes must be satisfied in order for angular momentum conservation to hold (Marshall 1981). The current form of the parameterization does not satisfy this constraint and hence further work is required to employ the parameterization in multiply-connected domains, e.g. with a circumpolar Southern Ocean. Additionally, we have specified that the eddy PV fluxes are directed down the mean PV gradient, which is true on average but may not hold locally. For example, up-gradient eddy PV fluxes are important in driving time-mean recirculation gyres in a wind-driven setup (Waterman and Hoskins 2013). Hence, there are important instances where the parameterization in its current form is not able to capture the full effect of the eddies on the mean flow.

There are further questions which remain to be addressed. We have shown that the parameterization can convert energy from eddy to mean, but it remains to be determined if it can also convert energy from mean to eddy in a sensible manner. Future work could determine this by testing the parameterization in a wind-driven gyre, in which the mean-to-eddy conversion is crucial in modulating the strength of the wind-driven jet (Waterman and Hoskins 2013). As mentioned previously, it is highly likely that the results of the parameterization depend on the representation of the terms in the energy and enstrophy budgets which we have not investigated here. Testing the parameterization with different iterations of energy and enstrophy budget may be useful in determining the effect of each on the resolved flow. Additionally, for simplicity, we have chosen to specify constant values for the parameters associated with the parameterization, but they will likely be variable in both space and time. We have not attempted to define the optimal choice of input parameters, nor have we specified what to optimize towards, since we have tested the parameterization in a highly idealised setup. Understanding of the key controls on the space-time variability of these parameters will be crucial in determining the optimal parameter set-up for a more realistic configuration.

Finally, we have so far implemented and tested the parameterization in a barotropic setup. How the parameterization should be implemented in a baroclinic setup remains to be determined. Future work could explore the extent to which the new parameterization can be included, alongside GM90, to represent the rectified forcing of the large-scale flow along topography contours by barotropic eddies.

*Acknowledgments.* Financial support was provided by the UK Natural Environment Research Council (NE/S007474/1) and the Oxford-Radciffe Scholarship. Collaboration was made possible by funding from University College Oxford and the Mitacs Globalink Research Award. Stephanie Waterman acknowledges funding from the Natural Sciences and Engineering Research Council of Canada (NSERC) Discovery Grants Program (NSERC-2020-05799). This work utilised the ARCHER2 UK National Supercomputing Service (https://www.archer2.ac.uk/).

*Data availability statement.* The code used for experiments discussed in this work can be found at https://github.com/rosieeaves/barotropic_model. Questions with regards to this code should be directed to Rosie Eaves.

## References

Adcock, S. T., and D. P. Marshall, 2000: Interactions between geostrophic eddies and the mean circulation over large-scale bottom topography. *J. Phys. Oceanogr.*, **30**, 3223–3238.

Arakawa, A., 1966: Computational design for long term numerical integration of the equations of fluid motion: two-dimensional incompressible flow. part i. *J. Comput. Phys.*, **1**, 119–143.

Arnold, V. I., 1965: Conditions for nonlinear stability of stationary plane curvilinear flows of an ideal fluid. *Dokl. Akad. Nauk. SSSR.*, **162**, 975–978.

Bachman, S. D., 2019: The gm+e closure: A framework for coupling backscatter with the gent and mcwilliams parameterization. *Ocean Modell.*, **136**, 85–106, https://doi.org/10.1016/j.ocemod.2019.02.006.

Bretherton, F. P., and D. B. Haidvogel, 1976: Two-dimensional turbulence above topography. *J. Fluid Mech.*, **78 (1)**, 129–154, https://doi.org/10.1017/S002211207600236X.

Cessi, P., 2008: An energy-constrained parameterization of eddy buoyancy flux. *J. Phys. Oceanogr.*, **38**, 1807–1819, https://doi.org/10.1175/2007JPO3812.1.

Danabasoglu, G., J. C. McWilliams, and P. R. Gent, 1994: The role of mesoscale tracer transports in the global ocean circulation. *Science*, **264**, 1123–1126.

Eby, M., and G. Holloway, 1994: Sensitivity of a large-scale ocean model to a parameterization of topographic stress. *J. Phys. Oceanogr.*, **24**, 2577–2588.

Eden, C., and R. J. Greatbatch, 2008: Towards a mesoscale eddy closure. *Ocean Modell.*, **20**, 223–239, https://doi.org/10.1016/j.ocemod.2007.09.002.

Eyring, V., S. Bony, G. A. Meehl, C. A. Senior, B. Stevens, R. J. Stouffer, and K. E. Taylor, 2016: Overview of the coupled model intercomparison project phase 6 (cmip6) experimental design and organization. *Geosci. Model Dev.*, **9**, 1937–1958, https://doi.org/10.5194/gmd-9-1937-2016.

Gent, P. R., and J. C. McWilliams, 1990: Isopycnal mixing in ocean circulation models. *J. Phys. Oceanogr.*, **20**, 150–155.

Green, J. S. A., 1970: Transfer properties of the large-scale eddies and the general circulation of the atmosphere. *Q. J. R. Meteorol. Soc.*, **96**, 157–185, https://doi.org/10.1002/qj.49709640802.

Gregory, J. M., and Coauthors, 2016: The flux-anomaly-forced model intercomparison project (fafmip) contribution to cmip6: Investigation of sea-level and ocean climate change in response to co2 forcing. *Geosci. Model Dev.*, **9**, 3993–4017, https://doi.org/10.5194/gmd-9-3993-2016.

Griffies, S. M., and Coauthors, 2009: Coordinated ocean-ice reference experiments (cores). *Ocean Modell.*, **26**, 1–46, https://doi.org/10.1016/j.ocemod.2008.08.007.

Griffies, S. M., and Coauthors, 2016: Omip contribution to cmip6: experimental and diagnostic protocol for the physical component of the ocean model intercomparison project. *Geosci. Model Dev.*, **9**, 3231–3296, https://doi.org/10.5194/gmd-9-3231-2016.

Holloway, G., 1992: Representing topographic stress for large-scale ocean models. *J. Phys. Oceanogr.*, **22 (9)**, 1033–1046, https://doi.org/10.1175/1520-0485(1992)022⟨1033:RTSFLS⟩2.0.CO;2.

Jansen, M. F., and I. M. Held, 2014: Parameterizing sub-grid scale eddy effects using energetically consistent backscatter. *Ocean Modell.*, **80**, 36–48, https://doi.org/10.1016/j.ocemod.2014.06.002.

Jones, C. D., and Coauthors, 2016: C4mip-the coupled climate-carbon cycle model intercomparison project: Experimental protocol for cmip6. *Geosci. Model Dev.*, **9**, 2853–2880, https://doi.org/10.5194/gmd-9-2853-2016.

Mana, P. P., and L. Zanna, 2014: Toward a stochastic parameterization of ocean mesoscale eddies. *Ocean Modell.*, **79**, 1–20, https://doi.org/10.1016/j.ocemod.2014.04.002.

Marshall, D. P., and A. J. Adcroft, 2010: Parameterization of ocean eddies: Potential vorticity mixing, energetics and arnold's first stability theorem. *Ocean Modell.*, **32**, 188–204, https://doi.org/10.1016/j.ocemod.2010.02.001.

Marshall, D. P., J. R. Maddison, and P. S. Berloff, 2012: A framework for parameterizing eddy potential vorticity fluxes. *J. Phys. Oceanogr.*, **42**, 539–557, https://doi.org/10.1175/JPO-D-11-048.1.

Marshall, D. P., R. G. Williams, and M.-M. Lee, 1999: The relation between eddy induced transport and isopycnic gradients of potential vorticity. *J. Phys. Oceanogr.*, **29**, 1571–1578, https://doi.org/10.1175/1520-0485(1999)029⟨1571:TRBEIT⟩2.0.CO;2.

Marshall, J. C., 1981: On the parameterization of geostrophic eddies in the ocean. *J. Phys. Oceanogr.*, **11**, 257–271.

Nazarenko, L., G. Holloway, and N. Tausnev, 1998: Dynamics of transport of "atlantic signature" in the arctic ocean. *J. Geophys. Res.*, **103**, 31 003–31 015, https://doi.org/10.1029/1998JC900017.

N, O. A., and P. E. Isachsen, 2003: The large-scale time-mean ocean circulation in the nordic seas and arctic ocean estimated from simplified dynamics. *J. Mar. Res.*, **61**, 175–210.

Rhines, P. B., 1975: Waves and turbulence on a beta-plane. *J. Fluid Mech.*, **69**, 417–443, https://doi.org/10.1017/S0022112075001504.

Tamarin, T., J. R. Maddison, E. Heifetz, and D. P. Marshall, 2016: A geometric interpretation of eddy reynolds stresses in barotropic ocean jets. *J. Phys. Oceanogr.*, **46**, 2285–2307, https://doi.org/10.1175/JPO-D-15-0139.1.

Wang, H., S. Legg, and R. Hallberg, 2018: The effect of arctic freshwater pathways on north atlantic convection and the atlantic meridional overturning circulation. *J. Climate*, **31**, 5165–5188, https://doi.org/10.1175/JCLI-D-17-0629.1.

Waterman, S., and B. J. Hoskins, 2013: Eddy shape, orientation, propagation, and mean flow feedback in western boundary current jets. *J. Phys. Oceanogr.*, **43**, 1666–1690, https://doi.org/10.1175/JPO-D-12-0152.1.

Zanna, L., P. P. Mana, J. Anstey, T. David, and T. Bolton, 2017: Scale-aware deterministic and stochastic parameterizations of eddy-mean flow interactions. *Ocean Modell.*, **111**, 66–80, https://doi.org/10.1016/j.ocemod.2017.01.004.